iScience

CellPress
OPEN ACCESS

Article

Sex differences in solute and water handling in the human kidney: Modeling and functional implications

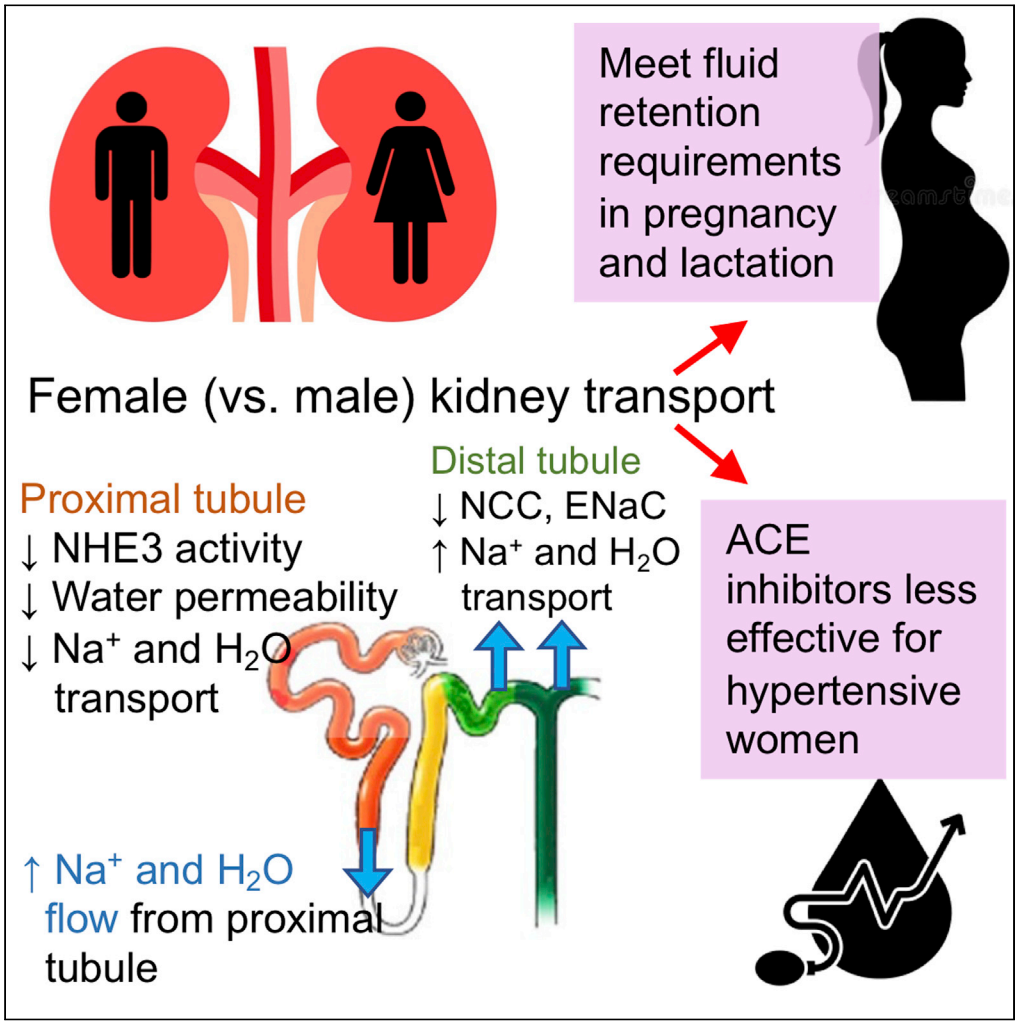

Rui Hu, Alicia A. McDonough, Anita T. Layton

anita.layton@uwaterloo.ca

Highlights

We have developed sex-specific models of solute and water transport in human kidneys

Human kidneys likely exhibit sexually dimorphic membrane transporter distribution

The pattern may prepare women for fluid retention required in pregnancy and lactation

The pattern may explain the lesser efficacy of ACE inhibitors in hypertensive women

Hu et al., iScience 24, 102667
June 25, 2021
https://doi.org/10.1016/j.isci.2021.102667

iScience

CellPress
OPEN ACCESS

Article

Sex differences in solute and water handling in the human kidney: Modeling and functional implications

Rui Hu,[1] Alicia A. McDonough,[2] and Anita T. Layton[1,3,4,*]

SUMMARY

The kidneys maintain homeostasis by controlling the amount of water and electrolytes in the blood. That function is accomplished by the nephrons, which transform glomerular filtrate into urine by a transport process mediated by membrane transporters. We postulate that the distribution of renal transporters along the nephron is markedly different between men and women, as recently shown in rodents. We hypothesize that the larger abundance of a renal Na^+ transport in the proximal tubules in females may also better prepare them for the fluid retention adaptations required during pregnancy and lactation. Also, kidneys play a key role in blood pressure regulation, and a popular class of anti-hypertensive medications and angiotensin converting enzymes (ACE) inhibitors have been reported to be less effective in women. Model simulations suggest that the blunted natriuretic and diuretic effects of ACE inhibition in women can be attributed, in part, to their higher distal baseline transport capacity.

INTRODUCTION

In addition to their function as filters, kidneys in mammals are specialized to serve various other essential regulatory functions, including water, electrolyte, and acid-base balance (Eaton and Pooler, 2009). In humans, each kidney contains about a million glomeruli, through which blood is filtered and becomes the tubular fluid of the nephron. The nephrons adjust the glomerular filtrate, via absorptive and secretive processes that are mediated by membrane transporters and channels on the renal tubular epithelial cells. Thus, tubular fluid begins at the glomerulus as an ultrafiltrate of plasma and is transformed into urine at the end of the nephrons (Eaton and Pooler, 2009). Regulation of the epithelial transport processes that match urine output to both intake of fluids and solutes, as well as to waste product production, is the subject of a large body of experimental and theoretical effort (Hoenig and Zeidel, 2014; Palmer and Schnermann, 2015; McDonough and Youn, 2017). Computational models have been developed to unravel the renal solute and water transport processes in humans (Layton and Layton, 2019; Hu and Layton 2021) and rats, under dietary (Weinstein, 2017; Layton et al., 2018) and therapeutic (Layton et al., 2015, 2016a; Layton and Vallon, 2018) manipulations, and under pathophysiological conditions (Layton et al., 2016b, 2017).

In recent years, a new dimension for investigation has emerged: sex. Like nearly every tissue and organ in the mammalian body, the structure and function of the kidney is regulated by sex hormones (Hatano et al., 2012; Hilliard et al., 2011; Sabolic et al., 2007; Sullivan and Gillis, 2017; Reckelhoff, 2001). Veiras et al. (Veiras et al., 2017) reported sexually dimorphic patterns in the abundance of electrolyte transporters, channels, and claudins (collectively referred to as transporters) in male and female rodents. Their findings demonstrated that, compared with male rat nephrons, female rat nephrons exhibit lower activities of major Na^+ and water transporters along the proximal portion of the renal tubule (proximal tubule), resulting in significantly larger fractional delivery of Na^+ and water to the downstream nephron segments in female kidneys. Along the distal nephron segments, the female kidney exhibits a higher abundance of key Na^+ transporters, relative to male, resulting in similar urine excretion between the sexes. To assess the functional implications of these findings, our group developed sex-specific rat nephron transport models (Hu et al., 2019, Hu et al., 2020; Li et al., 2018). Simulation results suggest an explanation for the more rapid excretion of a saline load in female rats observed in Ref (Veiras et al., 2017): In response to a saline load, the Na^+ load delivered distally is substantially greater in female rats than males, overwhelming transport capacity, cumulating in more rapid compensatory natriuresis in female rats.

[1]Department of Applied Mathematics, University of Waterloo, Waterloo, ON N2L 3G1, Canada

[2]Department of Physiology and Neuroscience, Keck School of Medicine, University of Southern California, Los Angeles, CA, USA

[3]Department of Biology, Cheriton School of Computer Science, and School of Pharmacology, University of Waterloo, Waterloo, ON N2L 3G1, Canada

[4]Lead contact

*Correspondence: anita.layton@uwaterloo.ca

https://doi.org/10.1016/j.isci.2021.102667

Some of these sex differences in rodent kidney function may translate to humans. Across race, men have higher blood pressure than women through much of lifespan (Stamler et al., 1976; Wenger et al., 2018). Given the essential role of the kidney in blood pressure control, sex differences in hypertension may be attributable, in part, to differences in kidney structure and function. That said, it is noteworthy that some significant differences in renal transporter patterns were reported between rats and mice (Veiras et al., 2017), and the differences between rat and human kidneys may be greater. For example, in rats, male kidneys are bigger than female kidneys, whereas men and women have kidneys of similar size (Emamian et al., 1993). Nonetheless, like female rats, women also face the challenge of circulating volume adaptation during pregnancy and lactation, and the potential for increasing reabsorption along the proximal nephron, coupled to the more abundant transporters in the distal nephron that may facilitate these adaptations. Given these observations, the objective of this study is to answer the questions: (1) To what extent can observed differences in blood pressure regulation between men and women be accounted for by sexual dimorphism in renal transporter patterns? (2) How do these differences in renal transporter pattern permit the reserve renal capacity that allows women to better handle the glomerular hyperfiltration that they face in pregnancy?

RESULTS

Sex differences in segmental transport under baseline conditions

The amounts of solutes and water reabsorbed or secreted along a given nephron segment depends, in part, on the activity of membrane transporters. We assume that human nephrons exhibit sexual dimorphism in membrane transporter patterns (density) similar to that observed in rats (Veiras et al., 2017). Unlike rats and mice, kidneys in men and women have similar size (Emamian et al., 1993), thus, similar effective tubular transport areas, as well as similar glomerular filtration rate (GFR) and urine output. Given the similarities in size and filtration between the human sexes, to what extent might sex differences in renal transporter expressions alter segmental solute and transport patterns? To answer that question, we conduct model simulations under control conditions and compare solute and water transport along individual segments in men and women. A schematic diagram for the model is shown in Figure 1.

Figure 2 shows the predicted delivery of key solutes [Na^+, K^+, Cl^-, HCO_3^-, NH_4^+, urea, and titratable acid (TA)] and fluid to the inlets of individual superficial and juxtamedullary nephron segments, expressed per kidney, in the male and female human models. [TA] is computed from [$H_2PO_4^+$] and [HPO_4^{2-}]. Single-nephron GFR (SNGFR) is assumed to be 100 and 133.3 nL/min in the superficial and juxtamedullary nephrons, respectively, in both sexes. Recall also that there are almost 6 times as many superficial than juxtamedullary nephrons, thus the smaller juxtamedullary contribution per kidney despite the higher SNGFR in the juxtamedullary nephrons (see Figure 2). Solute and fluid transport rates along individual superficial and juxtamedullary nephron segments are shown in Figure 3. Tubular fluid solute concentrations and luminal fluid flow are shown in Figures S1 and S2.

In both men and women, the majority of the filtered Na^+ is reabsorbed by the proximal tubules. In men, fractional Na^+ reabsorption is predicted to be 73%; in women, where the activity of the principal Na^+ transporter sodium hydrogen exchanger 3 (NHE3) is assumed to be 83% of men, which is 68%. Most of the remaining Na^+ is reabsorbed by the thick ascending limbs. With Na^+ delivery to the thick ascending limbs higher in women, we hypothesize that Na-K-Cl cotransporter (NKCC) activity is substantially higher in women (Table 1). Na-Cl cotransport (NCC) has been shown to be higher in women (Tahaei et al., 2020). With this configuration, Na^+ flows along the distal tubular segments are similar between men and women, as is urine Na^+ excretion, at ~0.6% of filtered Na^+ (Figures 2A and 3A). The transport of Cl^-, the accompanying anion, follows trends similar to Na^+ transport (Figures 2C and 3C).

Water transport is driven principally by the osmotic gradient; as such, along nephron segments that have sufficiently high water permeabilities, Na^+ reabsorption is accompanied by water reabsorption. The model predicts that 77% of the filtered volume is reabsorbed along the proximal tubules in men and 73% in women (Figures 2H and 3H). Because the thick ascending limbs have low water permeability, much of the Na^+ reabsorption along that segment is unaccompanied by water, resulting in a precipitous drop in tubular fluid osmolality from 700 at the inlet to 300 mosm/(kg H_2O) at the outflow of the thick ascending limbs. That substantial transcellular osmolality gradient, together with additional NaCl transport, drives water reabsorption along the water-permeable segments of the distal nephron. The model predicts that ~1% of the filtered volume is excreted.

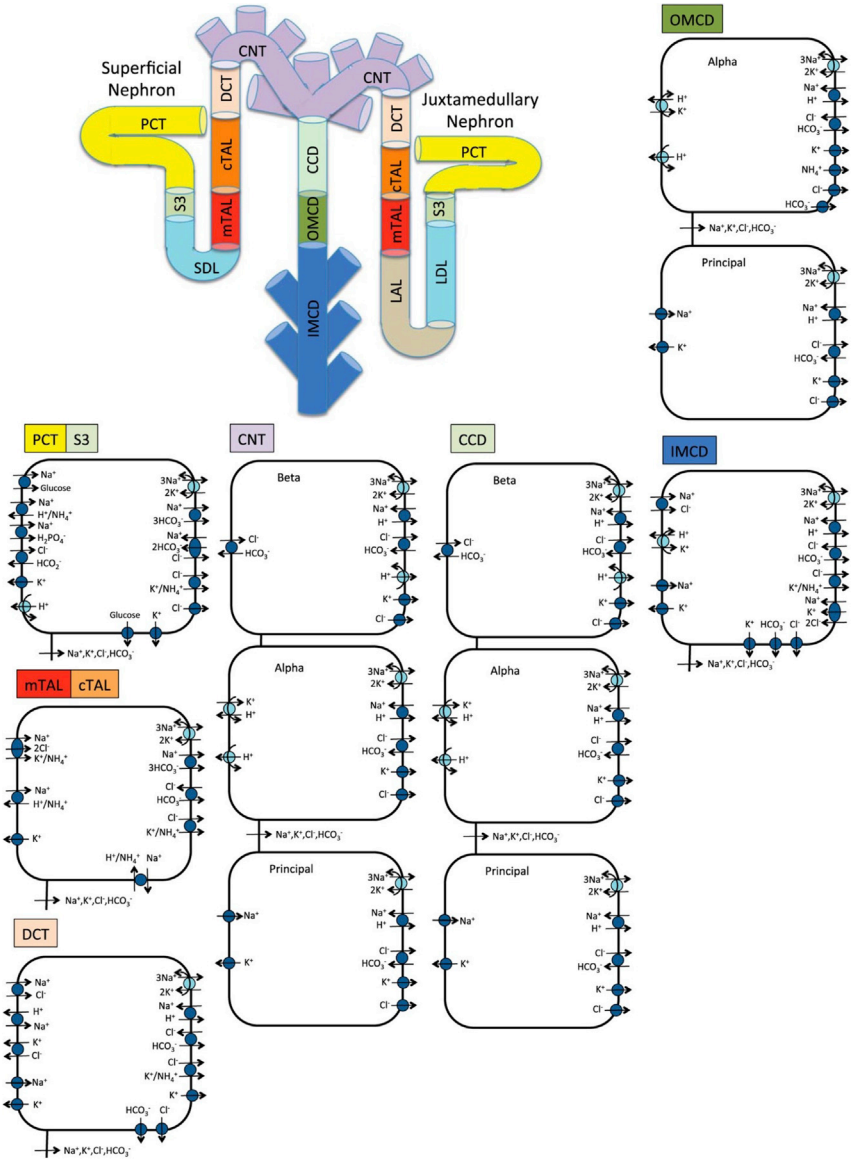

Figure 1. Schematic diagram of the nephron system (not to scale)

The model includes 1 representative superficial nephron and 5 representative juxtamedullary nephrons, each scaled by the appropriate population ratio. Only the superficial nephron and one juxtamedullary nephron are shown. Along each nephron, the model accounts for the transport of water and 15 solutes (see text). The diagram displays only the main Na^+, K^+, and Cl^- transporters. Red boxes highlight model membrane transporters whose expressions differ between males and females. mTAL, medullary thick ascending limb; cTAL, cortical thick ascending limb; DCT, distal convoluted tubule; PCT, proximal convoluted tubule; CNT, connecting duct; CCD, cortical collecting duct; SDL, short or outer-medullary descending limb; LDL/LAL, thin descending/ascending limb; OMCD, outer-medullary collecting duct; IMCD, inner-medullary collecting duct.

In terms of filtered K^+ loads, the model predicts that in men 68% of the filtered K^+ is reabsorbed along the proximal tubules, slightly higher than the 63% in women. The majority of the remaining K^+ is reabsorbed along the thick ascending limbs. Downstream of the Henle's loops, the model connecting tubules are assumed to vigorously secrete K^+. Owing to their longer length, juxtamedullary connecting tubules secrete substantially more K^+ than the superficial segments. Model parameters were chosen so that a similar fraction of the filtered K^+ load (16-17%) is excreted in men and women. See Figures 2B and 3B.

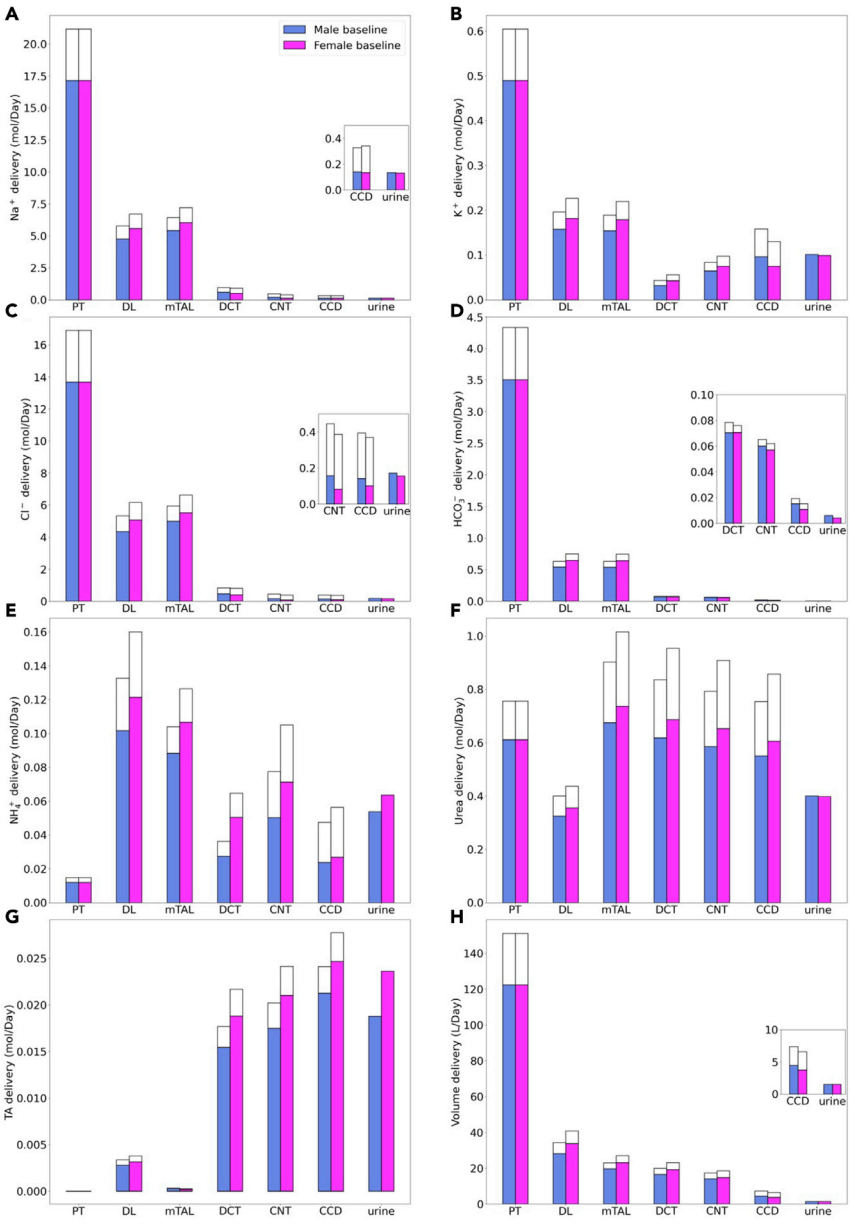

Figure 2. Segmental solute and water delivery

Delivery of key solutes (*A–G*) and fluid (*H*) to the beginning of individual nephron segments in men and women Color bars, superficial nephron values; white bars, juxtamedullary values, computed as weighed totals of the five representative model juxtamedullary nephrons. The model assumes a superficial-to-juxtamedullary nephron ratio of 85:15, thus, the superficial delivery values are generally higher. In each panel, the two bars for "urine" are identical since the superficial and juxtamedullary nephrons have merged at the cortical collecting duct entrance. PT, proximal tubule; DL, descending limb; mTAL, medullary thick ascending limb; DCT, distal convoluted tubule; CNT, connecting tubule; CCD, cortical collecting duct; TA, titratable acid. *Insets*: reproductions of distal segment values.

In both sexes, substantial NH_4^+ secretion occurs along the proximal tubules, via substitution of H^+ in the NHE3 transporter and secretion of NH_3. Downstream along the thick ascending limbs, a substantial fraction of NH_4^+ is reabsorbed substituting for K^+ in NKCC2. NH_4^+ excretion is predicted to be 19% higher in women (Figure 2E), consistent with the higher ammonia excretion reported in female mice, despite similar protein intake as males (Harris et al., 2018). Urea is reabsorbed along most nephron segments, except the

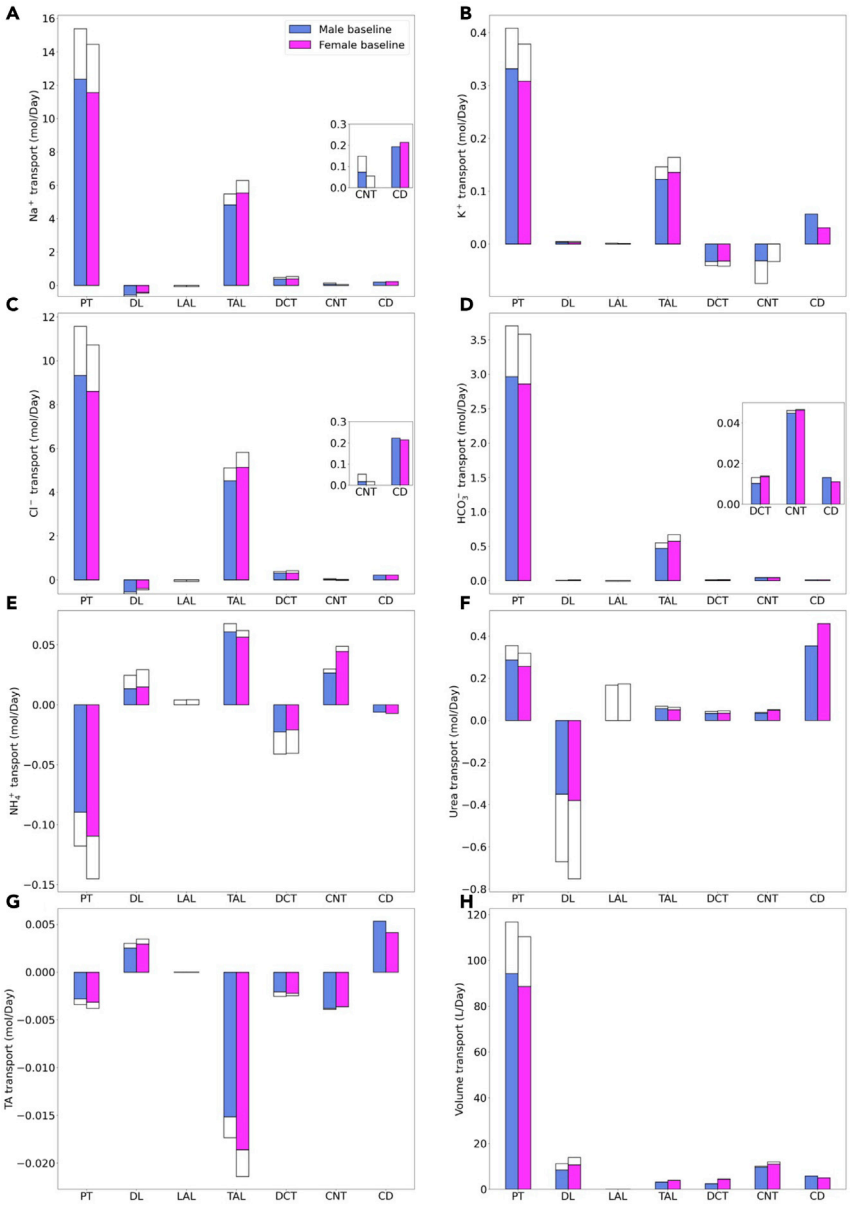

Figure 3. Segmental solute and water transport

Net transport of key solutes (A–G) along individual nephron segments, in men and women. Transport is taken positive out of a nephron segment. PT, proximal tubule; DL, descending limb; TAL, thick ascending limb; DCT, distal convoluted tubule; CNT, connecting tubule; CD, collecting duct; TA, titratable acid. Insets: reproductions of distal segment values. Notations are analogous to Figure 2.

descending limbs of the loops of Henle, where urea enters due to the presumed higher interstitial urea concentration (Figure 2F).

Female pattern provides renal transport reserve capacity necessary in to preserve water and salt in challenges of reproduction and lactation. The baseline simulations indicate that, given the same renal hemodynamics (input), renal transporter patterns in both men and women can yield similar urine excretion (output). The sex-specific transporter patterns indicate different segmental transport loads between the sexes. Nonetheless, the question remains: *Why should the transporter pattern be different between the sexes?* The answer may lie, in part, in the paradoxical NHE3 transport capacity observed in the rat proximal

Table 1. Key differences in nephron transport parameters between men and women.

Parameter	Female-male ratio		Parameter	Female-male ratio	
PCT:	Sup.	Jux.	S3:	Sup.	Jux.
NHE3 activity	0.83	0.83		0.83	0.83
NaPi2	0.75	0.75		0.75	0.75
P_{Na}, P_{Cl} (paracellular)	0.4	0.4		0.4	0.4
P_f (transcellular)	0.64	0.64		0.64	0.64
SDL:			LDL:		
P_{Na}, P_{Cl}(transcellular)	0.5				0.5
P_f (transcellular)	2				2
P_{Na}, P_{Cl} changing fraction					1.25
LAL:					
P_{Na}, P_{Cl}(transcellular)		2			
mTAL:			cTAL:		
NKCC activity	1.2	1.2		1.2	1.2
KCC activity	1.5	1.5		1.5	1.5
Na/K-ATPase activity	1.2	1.2		1.2	1.2
Na/H exchanger	0.8	0.8		0.8	0.8
Na/HPO_4 cotransporter	0.8	0.8		0.8	0.8
Na/HCO_3 cotransporter	0.8	0.8		0.8	0.8
P_{Na}, P_{Cl} (paracellular)	0.9	0.9			
DCT:			CNT:		
NCC activity	1.5	1.5			
Na/K-ATPase activity	1.5	1.5		1.5	1.5
Na/H exchanger	0.85	0.85		0.9	0.9
Na/HPO_4 cotransporter	0.85	0.85		0.9	0.9
ENaC activity	2	2		1.3	1.3
P_{Na}, P_{Cl} (paracellular)	1.4	1.4		1.4	1.4
P_f (transcellular)	2	2		1.5	1.5
CCD:			OMCD:		
Parameter	Female-male ratio		Parameter	Female-male ratio	
Na/K-ATPase activity	1.2			1.1	
H/K-ATPase activity	1			1.2	
Na/H exchanger	0.9			0.9	
Na/HPO_4 cotransporter	0.9			0.9	
ENaC activity	1.3			1.1	
P_{Na}, P_{Cl} (paracellular)	1.2			1	
P_K (transcellular)	0.7			1.2	
P_f (transcellular)	2			2	
IMCD:					

(*Continued on next page*)

Table 1. *Continued*

Parameter	Female-male ratio		Parameter	Female-male ratio	
PCT:	Sup.	Jux.	S3:	Sup.	Jux.
Na/K-ATPase activity	1.1				
H/K-ATPase activity	1.1				
K/Cl cotransporter	1.2				
NKCC1 activity	0.6				
P_{Na}, P_{Cl} (paracellular)	1.1				
P_K (transcellular)	1.4				
P_{Na} (transcellular)	1.5				
P_f (transcellular)	2				
P_{urea} changing fraction	0.89				

tubule (Veiras et al., 2017): NHE3 expression is higher in female compared to male rats, but NHE3 also exhibits a higher degree of phosphorylation, which is a marker for localization to the base of the microvilli and lower NHE3 activity (Brasen et al., 2014; Kocinsky et al., 2005). We hypothesize that the lower baseline proximal tubule NHE3 activity in females may represent reserve capacity that can be utilized to significantly increase reabsorption when presented with glomerular hyperfiltration in order to limit natriuresis and diuresis. For example, during pregnancy and lactation both GFR and tubular transport are increased without a corresponding rise in blood pressure (Munger and Baylis, 1988). To investigate this hypothesis, we conduct simulations in which we raise GFR and determine urine output under three settings: (i) baseline transport parameters in the kidney of a man, (ii) baseline transport parameters in the kidney of a woman (which we refer to as the "non-adaptive female model"), and (iii) renal transport parameters in a woman, with the reserve NHE3 transport capacity activated (which we refer to as the "adaptive female model").

Model simulations are limited to the consideration of glomerular hyperfiltration, tubular hypertrophy, and NHE3 activation; thus, these are by no means pregnancy/lactation simulations, even though some of the parameter choices are motivated by pregnancy-induced changes. In all three models, SNGFR is assumed to increase by 50% in superficial and 11% in juxtamedullary nephrons, consistent with GFR increases reported in pregnant women (Cheung and Lafayette, 2013). For the male and the non-adaptive female models, transport parameters are kept at baseline values (see (Layton and Layton, 2019) and Table 1). For the adaptive female model, we simulate the activation of reserve transport capacity by increasing NHE3 activity to 20% above male baseline value. Tubular hypertrophy is represented by increasing the model proximal tubule length by 20% (Garland et al., 1978). No other pregnancy-related renal transporter changes are represented as we aimed to focus on the impact of hemodynamics and proximal tubule NHE3 by asking: *Given increases in GFR similar to those observed in pregnancy, to what extent would the higher filtered load be compensated for in the female kidney with the proposed pregnancy-induced morphological and transport changes along the proximal tubules? And how does the resulting solute and water handling compare to the male and non-pregnant female kidneys?*

Predicted segmental solute and water deliveries are shown in Figure 4; segmental transport values are summarized in Figure S3. First compare the male and non-adaptive female models. The lower NHE3 activity in the non-adaptive female model results in 8% higher Na^+ delivery to the loops of Henle, compared to male. But the larger Na^+ transport capacity along the female thick ascending limbs and distal segments more than compensates; consequently, urinary Na^+ excretion is lower (22%) in the non-adaptive female model, compared to male (Figure 4).

Next, we consider the adaptive female model. The higher NHE3 activity and larger proximal transport area in the adaptive female kidney model results in a larger fraction of the filtered Na^+ and K^+ load being reabsorbed along the female proximal tubule compared to male (Figure S3). The difference in Na^+ flow (higher in the male model) is further augmented along downstream segments due to the higher (baseline) Na^+ capacity along the thick ascending limbs in the female models. Eventually, that results in urinary Na^+ excretion that is almost three times lower in women than in men (Figure 4).

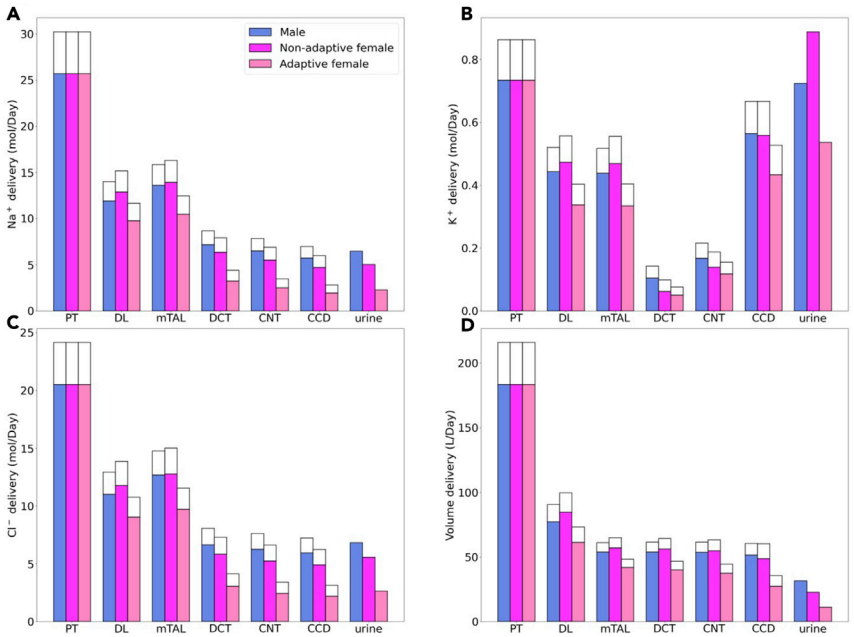

Figure 4. Effect of hemodynamic and PT changes on segmental delivery

Deliveries of key solutes (A–C) and fluid (D) to individual nephron segments, in male and female models 43% increase in GFR alone, and in the female model with 43% increase in GFR as well as NHE3 upregulation and PT hypertrophy and NHE3 upregulation. Delivery values are computed per kidney. Notations are analogous to Figure 2.

Despite the higher fractional reabsorption, the elevated GFR induces severe natriuresis, diuresis, and kaliuresis in all three models. The predicted Na^+ excretion is 17-, 38- and 47-fold higher than baseline in adaptive females, non-adaptive females and males, respectively. Because the reabsorption of Cl^- and water are largely coupled to Na^+, similar trends are obtained for the Cl^- excretion and urine output (Figure 4). The higher Na^+ flow increases tubular K^+ secretion in both sexes, resulting in markedly elevated K^+ excretion that is comparable to filtered K^+ load (Figure 4B).

Taken together, these simulations in men and women indicate that tubular hypertrophy, activation of reserve NHE3 capacity, and the higher (baseline) distal transport capacity together can attenuate the excessive natriuresis, diuresis, and kaliuresis that is predicted to arise due to hemodynamics changes similar to those observed in pregnancy. However, to achieve baseline urine output and excretion, additional changes are required, including transport adaptation along the distal segments (NP et al., 2008).

Female renal transporter pattern may explain sex differences in response to a class of anti-hypertensive medications. Sex differences are reported in the prevalence and severity of cardiorenal diseases, and in pharmacodynamics (Colafella and Denton, 2018; Falconnet et al., 2004). Of note is the angiotensin converting enzyme (ACE) inhibitors, a popular class of anti-hypertensive drugs target the renin-angiotensin system, which plays a key role in blood pressure regulation. ACE inhibitors lower blood pressure by reducing the production of angiotensin II (Ang II), a hormone that provokes vasoconstriction and fluid volume retention. ACE inhibitors are reported to be less effective in lowering blood pressure in women, compared to men (Falconnet et al., 2004; Zapater et al., 2004; Hudson et al., 2007; Sullivan, 2008). Given that Ang II acts along proximal and distal tubular segments to increase Na^+ transport, and thus, enhance salt and water retention, a reasonable question is: *To what extent can the lesser efficacy of ACE inhibitors' in women be explained by the sex differences in renal transporters, especially along the distal segments?*

To answer that question, we simulate ACE inhibition in men and women by decreasing NHE3 activity along the proximal tubule by 25%, by decreasing NKCC2 activity along the thick ascending limbs by 60%, and by decreasing the activities of NCC, NaK-ATPase, ROMK, and ENaC along distal convoluted tubule by 60%. ACE inhibition affects the proximal tubule, thick ascending limbs and downstream segments, and we assume that SNGFR is unchanged (McNabb et al., 1986; Vos et al., 1993). As noted above, because we assume

lower NHE3 activity, proximal Na^+ reabsorption is lower in women compared to men, resulting in higher NaCl and volume flow into the thick ascending limbs in women. Despite the higher Na^+ delivery to the thick ascending limbs, the lower NKCC2 activity, following ACE inhibition, results in a small increase in Na^+ reabsorption along the segment (~4%). In contrast, despite the reduction in NCC and ENaC activities along the distal segments, the higher tubular Na^+ flow increases Na^+ reabsorption, but to substantially different degrees in the two sexes. Owing to their higher distal transport capacity, Na^+ reabsorption increases by 52% in women, compared with only 31% in men. Similar effects are observed in water transport. Overall, ACE inhibition induces natriuresis and diuresis, but the increase in Na^+ excretion is about half in women relative to men; similarly, urine output increase is about two-thirds lower in women. These simulations suggest that the blunted natriuretic and diuretic effects of ACE inhibition in women can be attributed, in part, to their higher distal baseline transport capacity.

ACE inhibition affects most nephron segments. To dissect the impact of proximal versus distal inhibition by ACE, we conducted "proximal inhibition" simulations in which NHE3 activity was inhibited along the proximal tubule, and "distal inhibition" simulations in which NKCC2, NCC, NaK-ATPase, ROMK, and ENaC were inhibited along the downstream segments. Segmental delivery and transport of Na^+, K^+, Cl^-, and fluid are shown in Figures S4 and S5. Simulation results indicate a larger effect, in terms of urinary excretion, from proximal inhibition compared to distal.

DISCUSSION

The present study seeks to answer the question: What is the physiological implication of our postulated differences in renal membrane transporter distribution between men and women? Given that transport activity pattern is mostly uncharacterized in the human kidney, let alone the sex differences, we extrapolate our knowledge from rodents to humans. In the first modeling study of nephron transport in humans (Layton and Layton, 2019), we demonstrated that a model that combines known renal hemodynamics and morphological parameters in humans, with membrane solute and water transport parameters similar to rats, can predict segmental deliveries and urinary excretion of volume and key solutes that are consistent with human data. Transport parameters used in that human kidney modeling study (Layton and Layton, 2019) were based on the male rat. How might the results be different if we had modeled a woman by adopting transport parameters from the female rat (Veiras et al., 2017)?

In rats, baseline Na^+ transport of the proximal nephron is much lower in females, due to the significantly lower NHE3 activity and smaller tubular size. However, GFR and thus filtered load are also lower in females. In contrast, GFR is similar between men and women, as are their kidney size. Hence, in humans we focus on the renal transport pattern as the major contributor to any sex differences in nephron transport By assuming sexual dimorphisms similar to that in rats (Veiras et al., 2017), model simulations indicate that the lower fractional reabsorption of filtered Na^+ and water along the proximal nephron in women can be compensated by more abundant transporters, as well as the increased solute delivery to these transporters in downstream tubular segments (Figure 2), so that urine output and excretion rates are similar in men and women. It should be noted that the main proximal tubule sodium reabsorptive pathway, NHE3, is a Na^+/H^+ exchanger which contributes to acid excretion bicarbonate reabsorption and $NH4^+$ secretion. How sex differences in NHE3 and other transporters impact acid-base balance is a matter of current investigation by a number of labs (Harris et al., 2019). While it is reassuring that both the male and female renal transporter patterns can match urinary excretion to dietary intake, one may wonder why should the pattern be different between men and women in the first place? A notable sex difference observed in rats, that we assume translates to humans, is that NHE3 is actually more abundant along the proximal tubules in females, but a larger fraction of NHE3 is phosphorylated and thus inactive. In other words, females appear to have a larger proximal Na^+ transport reserve. Additionally, Na^+ transport along the distal nephron is exquisitely regulated, and its larger contribution to total renal Na^+ transport in females may also better prepare them for the fluid retention adaptations required during pregnancy and lactation.

Pregnancy involves a remarkable orchestration of changes in the majority of the physiological systems, including essentially all aspects of kidney function. Mild increases in proteinuria, glucosuria, lower serum osmolality, and reductions in serum Na^+ levels are often reported in pregnancy (Davison et al., 1988; Schrier, 2010; Kuo et al., 1992). Renal and systemic hemodynamics are both drastically altered by the marked volume expansion and vasodilation. As such, renal plasma flow increases by up to 80% and GFR increases by 50% (Dunlop, 1981). Does the female renal transporter pattern better prepare women to

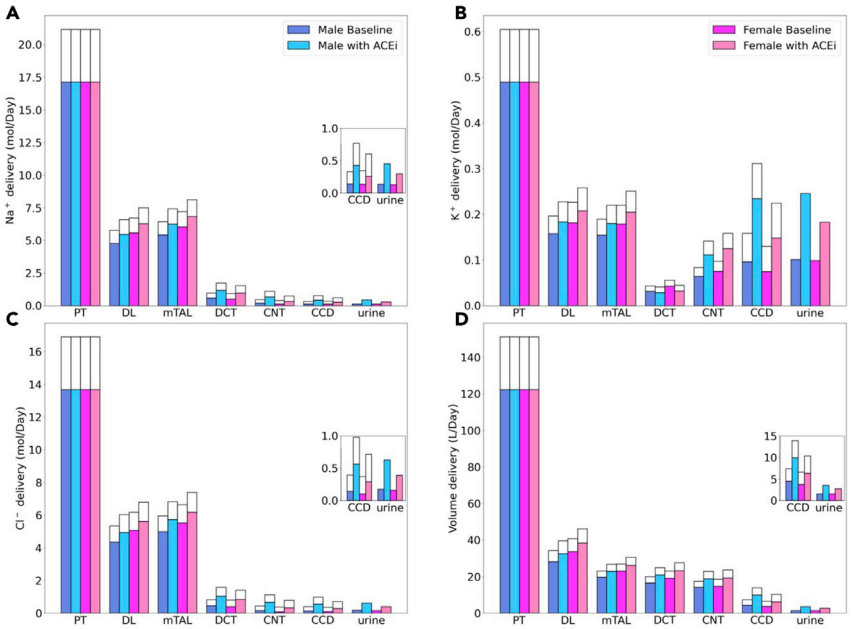

Figure 5. Segmental delivery under ACE inhibition

Comparison of solute delivery (*A–C*) and fluid delivery (*D*) obtained for base case and for ACE inhibition for both sexes. Delivery values are computed per kidney. Notations are analogous to Figure 2.

handle the much larger filtered load? Model simulations indicate that by dephosphorylating and thereby activating the reserve NHE3 in the proximal nephron, the female human kidney can limit excessive natriuresis and diuresis, compared to males (see Figure 4) and also indicate that the larger transport capacity in the distal nephron of the female kidney renders women better equipped to handle (i.e., retain a significantly more of) the larger filtered load in pregnancy. Nevertheless, to completely compensate for the heightened load in pregnancy, further alternations in tubular transport are required (NP et al., 2008; West et al., 2015; West et al., 2018).

The kidney plays an indispensable role in blood pressure regulation (Cowley, 1992). To maintain arterial circulation and blood pressure, the kidney tightly controls its own renal perfusion pressure, renal perfusion, and extracellular volume. Renal artery perfusion pressure directly regulates sodium excretion, in a process known as pressure natriuresis, and influences the activity of various vasoactive systems such as the renin-angiotensin system (RAS). Major differences are evident between men and women in the RAS that may manifest in differences in blood pressure regulation (Sandberg and Ji, 2003; Sullivan, 2008). Indeed, the prevalence of hypertension is higher in men than in women prior to the onset of menopause.

Historically, most epidemiological and experimental data collected on the progression of hypertension and chronic renal disease were collected in men, as were data on the effectiveness of therapeutic interventions. Few clinical trials examining the health benefits of RAS inhibition have reported data for both sexes separately, even when women have been included. Falconnet et al. reported that, following a 20-day treatment with lisinopril at 20 mg/day, men responded with a larger decrease in ambulatory blood pressure compared with women (Falconnet et al., 2004). Their data suggest that over time, the effectiveness of ACE inhibition is lessened in women. That conclusion is supported by additional cardiovascular studies in patients with congestive heart failure and following myocardial infarction in which ACE inhibition confers less cardiovascular benefit to women compared with men as assessed by total mortality (Hudson et al., 2007). *To which extent can the sex differences in the response to ACE inhibitors be attributable to sex differences in renal tubular transport?* To answer this question, we simulated kidney function following ACE inhibition, and compared the predicted natriuretic and diuretic responses in men and women. We assumed that ACE inhibition generates the same fractional reduction in key Na^+ transporter activities in men and women. With this key assumption, model simulations suggest that the higher distal transport capacity in women results in greater attenuation in natriuresis and diuresis, than in men (Figure 5), which, when taken

in isolation, may result in a small reduction in blood pressure. In male rodents, angiotensin II stimulates and ACE inhibitors attenuates proximal tubule Na^+ reabsorption through actions on NHE3 and Na,K-ATPase (Leong et al., 2006; Massey et al., 2016). While similar studies in females are, to our knowledge, lacking, the lesser sodium reabsorption in female versus male rats indicates that ACE inhibitors would have more proximal sodium transport to inhibit in males than in females. While these results suggest that sex differences in tubular transport may contribute to the lesser efficacy of ACE inhibitors in women, one must not neglect the other systems that are affected by or interact with the action of ACE inhibitors (Taddei and Bortolotto, 2016).

In sum, we have extended our work in sex-specific modeling of kidney function in the rat (Hu et al., 2019, Hu et al., 2020; Li et al., 2018; Chen et al., 2017; Ahmed and Layton, 2020) to human. Compared to rodents, human kidneys are more similar between the sexes, in terms of morphology and hemodynamics. Nonetheless, our study suggests that sexual dimorphism in renal transport pattern similar to that reported in rodent may better prepare women for the heightened demands on the kidney during pregnancy and may also contribute to the two sexes' differential response to ACE inhibition. The present sex-specific nephron models can be used as essential components in more comprehensive models of integrated kidney function. For instance, computational models of whole-body blood pressure regulation typically include a highly simplified representation of the kidney (e.g. (Hallow et al., 2014; Leete and Layton, 2019)). Incorporating elaborate sex-specific nephron transport models would allow more accurate simulations of the very commonly prescribed anti-hypertensive treatments that target the kidney (e.g., ACE inhibitors, diuretics) and analysis of any sex differences in drug efficacy. The present model can be combined with models of renal oxygenation that represent blood flow and tubular metabolism (Chen et al., 2010; Fry et al., 2014, 2015, 2016; Lee et al., 2017, 2018). The resulting comprehensive sex-specific models of kidney oxygenation would allow one to conduct a comprehensive *in silico* study of factors that give rise to the impact of sex on the progression of chronic kidney disease (Silbiger and Neugarten, 1995).

It has become increasingly clear that experimental and clinical results obtained in one sex cannot be extrapolated to both sexes without sufficient justification. A better understanding of the sex differences in renal physiology and pathophysiology is a necessary step toward a true understanding of the complicated transport and excretion processes in the kidney, and, if needed, toward sex-specific and more effective therapeutic treatments for men and women.

Limitations of the study

The laboratory rat is arguably one of the most well studied animals. In particular, many of the morphological and molecular properties of its kidney have been experimentally measured. As such, computational models of the kidney have traditionally been based on the rat. However, the clinical value of these models is limited, an observation that motivated us to begin developing the computational models of the human kidney, first for men (Layton and Layton, 2019), and in the present study for women as well. Unlike the rat, renal transport activity pattern is mostly uncharacterized in the human kidney, let alone the sex differences. We extrapolated and adjusted rodent data humans. Thus, while a human kidney model offers a valuable platform for *in silico* biomedical research, the substantial uncertainty in model parameters must be acknowledged.

In our simulations, we assume that ACE inhibition has the same effect on kidney transport in men and women. However, major sex differences in the RAS have been identified, including how much substrate is produced and how angiotensin interacts with receptors. For example, in both rats and humans, females have greater circulating levels of AGT (Fischer et al., 2002), causing an overall greater amount of angiotensin to be flowing through the system. In addition, male rats have been shown to have greater Ang II levels (Sandberg and JI, 2012) while female rats have greater levels of Ang (1–7) (Zimmerman and Sullivan, 2013). However, a greater level of ACE2 activity (which converts Ang II to Ang (1–7)) has been measured in male rats (Zimmerman and Sullivan, 2013). Indeed, males and females exhibit differing responses to Ang II. Changes in Ang II levels produce smaller changes in blood pressure in female rats (Fischer et al., 2002, Sandberg and JI, 2012). This discrepancy may be attributed to differences in receptor expression, inasmuch as male rats have greater AT1R expression and lower AT2R expression than female rats (Bubb et al., 2012; Sandberg and JI, 2012; Zimmerman and Sullivan, 2013). Estrogen also reduces the half-life of AT1R-bound Ang II (Thompson and Khalil, 2003). Given the above observations, it is likely that ACE inhibitors affect

nephron transport differently in men and women, but those effects have not been sufficiently well characterized.

STAR★METHODS

Detailed methods are provided in the online version of this paper and include the following:

- KEY RESOURCES TABLE
- RESOURCE AVAILABILITY
  - Lead contact
  - Materials availability
  - Data and code availability
- METHOD DETAILS
  - Key model equations

SUPPLEMENTAL INFORMATION

Supplemental information can be found online at https://doi.org/10.1016/j.isci.2021.102667.

ACKNOWLEDGMENT

This research was supported by the Canada 150 Research Chair program, by the Natural Sciences and Engineering Research Council of Canada, via a Discovery award to ATL, and by the National Institutes of Health NIDDK, via 2R01DK083785 and R56DK123780 to AAMcD.

AUTHOR CONTRIBUTIONS

Conceptualization, A.T.L.; methodology, A.T.L.; software, R.H. and A.T.L.; formal analysis, R.H. and A.T.L.; investigation, R.H. and A.T.L.; data curation, R.H. and A.T.L.; writing–original draft, A.T.L.; writing–review & editing, R.H., A.A.M., and A.T.L.; visualization, R.H. and A.T.L.; funding acquisition, A.A.M. and A.T.L.

DECLARATION OF INTERESTS

The authors declare no competing interests.

Received: May 4, 2021
Revised: May 19, 2021
Accepted: May 26, 2021
Published: June 25, 2021

REFERENCES

Ahmed, S., and Layton, A.T. (2020). Sex-specific computational models for blood pressure regulation in the rat. Am. J. Physiol. Ren. Physiol. *318*, F888–F900.

Brasen, J.C., Burford, J.L., Mcdonough, A.A., Holstein-Rathlou, N.H., and Peti-Peterdi, J. (2014). Local pH domains regulate NHE3-mediated Na(+) reabsorption in the renal proximal tubule. Am. J. Physiol. Ren. Physiol. *307*, F1249–F1262.

Bubb, K.J., Khambata, R.S., and Ahluwalia, A. (2012). Sexual dimorphism in rodent models of hypertension and atherosclerosis. Br. J. Pharmacol. *167*, 298–312.

Chen, J., Edwards, A., and Layton, A.T. (2010). Effects of pH and medullary blood flow on oxygen transport and sodium reabsorption in the rat outer medulla. Am. J. Physiol. Renal Physiol. *298*, F1369–F1383.

Chen, Y., Sullivan, J.C., Edwards, A., and Layton, A.T. (2017). Sex-specific computational models of the spontaneously hypertensive rat kidneys: factors affecting nitric oxide bioavailability. Am. J. Physiol. Ren. Physiol *313*, F174–F183.

Cheung, K.L., and Lafayette, R.A. (2013). Renal physiology of pregnancy. Adv. Chronic Kidney Dis. *20*, 209–214.

Colafella, K.M.M., and Denton, K.M. (2018). Sex-specific differences in hypertension and associated cardiovascular disease. Nat. Rev. Nephrol. *14*, 185–201.

Cowley, A.W., Jr. (1992). Long-term control of arterial blood pressure. Physiol. Rev. *72*, 231–300.

Davison, J.M., Shiells, E.A., Philips, P.R., and Lindheimer, M. (1988). Serial evaluation of vasopressin release and thirst in human pregnancy. Role of human chorionic gonadotrophin in the osmoregulatory changes of gestation. J. Clin. Invest. *81*, 798–806.

Dunlop, W. (1981). Serial changes in renal haemodynamics during normal human pregnancy. Br. J. Obstet. Gynaecol. *88*, 1–9.

Eaton, D.C., and Pooler, J.P. (2009). Vander's renal physiology (Mc Graw Hil Medicall).

Emamian, S.A., Nielsen, M.B., Pedersen, J.F., and Ytte, L. (1993). Kidney dimensions at sonography: correlation with age, sex, and habitus in 665 adult volunteers. Am. J. Roentgenol. *160*, 83–86.

Falconnet, C., Bochud, M., Bovet, P., Maillard, M., and Burnier, M. (2004). Gender difference in the response to an angiotensin-converting enzyme inhibitor and a diuretic in hypertensive patients of African descent. J. Hypertens. *22*, 1213–1220.

Fischer, M., Baessler, A., and Schunkert, H. (2002). Renin angiotensin system and gender differences in the cardiovascular system. Cardiovasc. Res. *53*, 672–677.

Fry, B.C., Edwards, A., and Layton, A.T. (2015). Impacts of nitric oxide and superoxide on renal medullary oxygen transport and urine concentration. Am. J. Physiol. Ren. Physiol. *308*, F967–F980.

Fry, B.C., Edwards, A., and Layton, A.T. (2016). Impact of nitric-oxide-mediated vasodilation and oxidative stress on renal medullary oxygenation: a modeling study. Am. J. Physiol. Ren. Physiol. *310*, F237–F247.

Fry, B.C., Edwards, A., Sgouralis, I., and Layton, A.T. (2014). Impact of renal medullary three-dimensional architecture on oxygen transport. Am. J. Physiol. Ren. Physiol. *307*, F263–F272.

Garland, H., Green, R., and Moriarty, R. (1978). Changes in body weight, kidney weight and proximal tubule length during pregnancy in the rat. Kidney Blood Press. Res. *1*, 42–47.

Hallow, K.M., Lo, A., Beh, J., Rodrigo, M., Ermakov, S., Friedman, S., De Leon, H., Sarkar, A., Xiong, Y., Sarangapani, R., et al. (2014). A model-based approach to investigating the pathophysiological mechanisms of hypertension and response to antihypertensive therapies: extending the Guyton model. Am. J. Physiol. Regul. Integr. Comp. Physiol. *306*, R647.

Harris, A.N., Lee, H.-W., Fang, L., Verlander, J.W., and Weiner, I.D. (2019). Differences in acidosis-stimulated renal ammonia metabolism in the male and female kidney. Am. J. Physiol. Ren. Physiol. *317*, F890–F905.

Harris, A.N., Lee, H.W., Osis, G., Fang, L., Webster, K.L., Verlander, J.W., and Weiner, I.D. (2018). Differences in renal ammonia metabolism in male and female kidney. Am. J. Physiol. Ren. Physiol. *315*, F211–F222.

Hatano, R., Onoe, K., Obara, M., Matsubara, M., Kanai, Y., Muto, S., and Asano, S. (2012). Sex hormones induce a gender-related difference in renal expression of a novel prostaglandin transporter, OAT-PG, influencing basal PGE2 concentration. Am. J. Physiol. Ren. Physiol. *302*, F342–F349.

Hilliard, L.M., Nematbakhsh;, M., Kett, M.M., Teichman;, E., Sampson, A.K., Widdop, R.E., Evans;, R.G., and Denton, K.M. (2011). Gender differences in pressure-natriuresis and renal autoregulation: role of the angiotensin type 2 receptor. Hypertension *57*, 275–282.

Hoenig, M.P., and Zeidel, M.L. (2014). Homeostasis, the milieu interieur, and the wisdom of the nephron. Clin. J. Am. Soc. Nephrol. *9*, 1272–1281.

Hu, R., and Layton, A. (2021). A computational model of kidney function in a patient with diabetes. Int. J. Mol. Sci. *22*, 5819.

Hu, R., Mcdonough, A.A., and Layton, A.T. (2019). Functional implications of the sex differences in transporter abundance along the rat nephron: modeling and analysis. Am. J. Physiol. Ren. Physiol. *317*, F1462–F1474.

Hu, R., Mcdonough, A.A., and Layton, A.T. (2020). Sex-differences in solute transport along the nephrons: effects of Na+ transport inhibition. Am. J. Physiol. Ren. Physiol. *319*, F487–F505.

Hudson, M., Rahme, E., Behlouli, H., Sheppard, R., and Pilote, L. (2007). Sex differences in the effectiveness of angiotensin receptor blockers and angiotensin converting enzyme inhibitors in patients with congestive heart failure–a population study. Eur. J. Heart Fail. *9*, 602–609.

Kocinsky, H., Girardi, A., Biemesderfer, D., Nguyen, T., Mentone, S., Orlowski, J., and Aronson, P. (2005). Use of phospho-specific antibodies to determine the phosphorylation of endogenous Na+/H+ exchanger NHE3 at PKA consensus sites. Am. J. Physiol. Ren. Physiol. *289*, F249–F258.

Kuo, V.S., Koumantakis, G., and Gallery, E.D. (1992). Proteinuria and its assessment in normal and hypertensive pregnancy. Am. J. Obstet. Gynecol. *167*, 723–728.

Layton, A.T., Aurélie Edwards, A., and Vallon, V. (2018). Renal potassium handling in rats with subtotal nephrectomy: modeling and analysis. Am. J. Physiol. Ren. Physiol. *314*, F643–F657.

Layton, A.T., Laghmani, K., Vallon, V., and Edwards, A. (2016a). Solute transport and oxygen consumption along the nephrons: effects of Na+ transport inhibitors. Am. J. Physiol. Ren. Physiol. *311*, F1217–F1229.

Layton, A.T., and Layton, H.E. (2019). A computational model of epithelial solute and water transport along a human nephron. PLoS Comput. Biol. *15*, e1006108.

Layton, A.T., and Vallon, V. (2018). SGLT2 inhibition in a kidney with reduced nephron number: modeling and analysis of solute transport and metabolism. Am. J. Physiol. Ren. Physiol. *314*, F969–F984.

Layton, A.T., Vallon, V., and Edwards, A. (2015). Modeling oxygen consumption in the proximal tubule: effects of NHE and SGLT2 inhibition. Am. J. Physiol. Ren. Physiol. *308*, F1343–F1357.

Layton, A.T., Vallon, V., and Edwards, A. (2016b). Predicted consequences of diabetes and SGLT inhibition on transport and oxygen consumption along a rat nephron. Am. J. Physiol. Ren. Physiol. *310*, F1269–F1283.

Layton, A.T., Vallon, V., and Edwards, A. (2017). Adaptive changes in GFR, tubular morphology and transport in subtotal nephrectomized kidneys: modeling and analysis. Am. J. Physiol. Ren. Physiol. *313*, F199–F209.

Lee, C.-J., Gardiner, B.S., Evans, R.G., and Smith, D.W. (2018). A model of oxygen transport in the rat renal medulla. Am. J. Physiol. Ren. Physiol. *315*, F1787–F1811.

Lee, C.-J., Gardiner, B.S., Ngo, J.P., Kar, S., Evans, R.G., and Smith, D.W. (2017). Accounting for oxygen in the renal cortex: a computational study of factors that predispose the cortex to hypoxia. Am. J. Physiol. Ren. Physiol. *313*, F218–F236.

Leete, J., and Layton, A.T. (2019). Sex-specific long-term blood pressure regulation: modeling and analysis. Comput. Biol. Med. *104*, 139–148.

Leong, P.K., Devillez, A., Sandberg, M.B., Yang, L.E., Yip, D.K., Klein, J.B., and Mcdonough, A.A. (2006). Effects of ACE inhibition on proximal tubule sodium transport. Am. J. Physiol. Ren. Physiol. *290*, F854–F863.

Li, Q., Mcdonough, A.A., Layton, H.E., and Layton, A.T. (2018). Functional implications of sexual dimorphism of transporter patterns along the rat proximal tubule: modeling and analysis. Am. J. Physiol. Ren. Physiol. *315*, F692–F700.

Massey, K.J., Li, Q., Rossi, N.F., Keezer, S.M., Mattingly, R.R., and Yingst, D.R. (2016). Phosphorylation of rat kidney Na-K pump at Ser938 is required for rapid angiotensin II-dependent stimulation of activity and trafficking in proximal tubule cells. Am. J. Physiol. Ren. Physiol. *310*, C227–C232.

McDonough, A.A., and Youn, J.H. (2017). Potassium homeostasis: the knowns, the unknowns, and the health benefits. Physiology *32*, 100–111.

McNabb, W.R., Noormohamed, F.H., and Lant, A.F. (1986). The effects of enalapril on blood pressure and the kidney in normotensive subjects under altered sodium balance. J. Hypertens. *4*, 39–47.

Munger, K., and Baylis, C. (1988). Sex differences in renal hemodynamics in rats. Am. J. Physiol. *254*, F223–F231.

NP, A., Tardin, J.C.B.M., Boim, M.A., Campos, R.R., Bergamaschi, C.T., and Schor, N. (2008). Hemodynamic parameters during normal and hypertensive pregnancy in rats: evaluation of renal salt and water transporters. Hypertens. Pregnancy *27*, 49–63.

Oliver, J. (1968). Nephrons and Kidneys: A Qualitative Study of Development and Evolutionary Mammalian Renal Architecture (Harper and Row).

Palmer, L.G., and Schnermann, J. (2015). Integrated control of Na transport along the nephron. Clin. J. Am. Soc. Nephrol. *10*, 676–687.

Reckelhoff, J.F. (2001). Gender differences in the regulation of blood pressure. Hypertension *37*, 1199–1208.

Sabolic, I., Asif, A.R., Budach, W.E., Wanke, C., Bahn, A., and Burckhardt, G. (2007). Gender differences in kidney function. Pflugers Arch. *455*, 397–429.

Sabolic, I., Vrhovac, I., Eror, D.B., Gerasimova, M., Rose, M., Breljak, D., Ljubojevic, M., Brzica, H., Sebastiani, A., Thal, S.C., et al. (2012). Expression of Na+-D-glucose cotransporter SGLT2 in rodents is kidney-specific and exhibits sex and species differences. Am. J. Physiol. Ren. Physiol. *302*, C1174–C1188.

Sandberg, K., and Ji, H. (2003). Sex and the renin angiotensin system: implications for gender differences in the progression of kidney disease. Adv. Ren. Replace Ther. *10*, 15–23.

Sandberg, K., and JI, H. (2012). Sex differences in primary hypertension. Biol. Sex Differ. *3*, 1–12.

Schrier, R.W. (2010). Systemic arterial vasodilation, vasopressin, and vasopressinase in pregnancy. J. Am. Soc. Nephrol. *21*, 570–572.

Silbiger, S.R., and Neugarten, J. (1995). The impact of gender on the progression of chronic renal disease. Am. J. Kidney Dis. *25*, 515–533.

Stamler, J., Stamler, R., Riedlinger, W.F., Algera, G., and Roberts, R.H. (1976). Hypertension screening of 1 million Americans: community hypertension evaluation clinic (CHEC) program, 1973 through 1975. Jama *235*, 2299–2306.

Sullivan, J.C. (2008). Sex and the renin-angiotensin system: inequality between the sexes in response to RAS stimulation and inhibition. Am. J. Physiol. Regul. Integr. Comp. Physiol. *294*, R1220–R1226.

Sullivan, J.C., and Gillis, E.E. (2017). Sex and gender differences in hypertensive kidney injury. Am. J. Physiol. Ren. Physiol. *313*, F1009–F1017.

Taddei, S., and Bortolotto, L. (2016). Unraveling the pivotal role of bradykinin in ACE inhibitor activity. Am. J. Cardiovasc. Drugs *16*, 309–321.

Tahaei, E., Coleman, R., Saritas, T., Ellison, D.H., and Welling, P.A. (2020). Distal convoluted tubule sexual dimorphism revealed by advanced 3D imaging. Am. J. Physiol. Ren. Physiol. *319*, F754–F764.

Thompson, J., and Khalil, R.A. (2003). Gender differences in the regulation of vascular tone. Clin. Exp. Pharmacol. Physiol. *30*, 1–15.

Veiras, L.C., Girardi, A.C.C., Curry, J., Pei, L., Ralph, D.L., Tran, A., Castelo-Branco, R.C., Pastor-Soler, N., Arranz, C.T., Yu, A.S.L., and Mcdonough, A.A. (2017). Sexual dimorphic pattern of renal transporters and electrolyte homeostasis. J. Am. Soc. Nephrol. *28*, 3504–3517.

Vos, P., Boer, P., and Koomans, H. (1993). Effects of enalapril on renal sodium handling in healthy subjects on low, intermediate, and high sodium intake. J. Cardiovasc. Pharmacol. *22*, 27–32.

Weinstein, A.M. (2017). A mathematical model of the rat kidney: K(+)-induced natriuresis. Am. J. Physiol. Ren. Physiol *312*, F925–F950.

Wenger, N.K., Arnold, A., Merz, C.N.B., Cooper-Dehoff, R.M., Ferdinand, K.C., Fleg, J.L., Gulati, M., Isiadinso, I., Itchhaporia, D., and Light-Mcgroary, K. (2018). Hypertension across a woman's life cycle. J. Am. Coll. Cardiol. *71*, 1797–1813.

West, C.A., Verlander, J.W., Wall, S.M., and Baylis, C. (2015). The chloride–bicarbonate exchanger pendrin is increased in the kidney of the pregnant rat. Exp. Physiol. *100*, 1177–1186.

West, C.A., Welling, P.A., West, D.A., Jr., Coleman, R.A., Cheng, K.-Y., Chen, C., Dubose, T.D., Jr., Verlander, J.W., Baylis, C., and Gumz, M.L. (2018). Renal and colonic potassium transporters in the pregnant rat. Am. J. Physiol. Ren. Physiol. *314*, F251–F259.

Zapater, P., Novalbos, J., Gallego-Sandín, S., Hernández, F.T., and Abad-Santos, F. (2004). Gender differences in angiotensin-converting enzyme (ACE) activity and inhibition by enalaprilat in healthy volunteers. J. Cardiovasc. Pharmacol. *43*, 737–744.

Zimmerman, and Sullivan, J.C. (2013). Hypertension: what's sex got to do with it? Physiology *28*, 234–244.

STAR★METHODS

KEY RESOURCES TABLE

REAGENT or RESOURCE	SOURCE	IDENTIFIER
Software and Algorithms		
Computer code	This study	https://github.com/uwrhu/Python-nephron-model-parallel-code

RESOURCE AVAILABILITY

Lead contact

Further information and requests for resources should be directed to the lead contact, Anita Layton (anita.layton@uwaterloo.ca).

Materials availability

This study did not generate new unique reagents or other new materials.

Data and code availability

The code generated in this study can be accessed via https://github.com/uwrhu/Python-nephron-model-parallel-code. See key resources table.

METHOD DETAILS

We previously developed an epithelial cell-based model of solute transport along a superficial nephron of a human (male) kidney (Layton and Layton, 2019). That human kidney model was formulated by combining published human hemodynamic and morphological data with the published transporter expression data in rats. In this study, we extend that model (i) to include the juxtamedullary nephron populations, and (ii) to represent nephron populations in a woman's kidney. (Superficial nephrons turn at the outer-inner medullary boundary, whereas juxtamedullary nephrons reach into differing levels of the inner medulla.) The model represents six classes of nephrons: a superficial nephron (denoted "SF") and five juxtamedullary nephrons (denoted "JM"). The superficial nephrons account for 85% of the nephron population, and extend from the Bowman's capsule to the papillary tip. The remaining 15% of the nephrons are juxtamedullary that possess loops of Henle that reach to different depths in the inner medulla; most of the long loops turn within the upper inner medulla. The model nephron is represented as a tubule lined by a layer of epithelial cells, with apical and basolateral transporters that vary according to cell type. The model assumes that the connecting tubules coalesce successively within the cortex, resulting in a ratio of loop-to-cortical collecting duct of 10:1 (Oliver, 1968). In the inner medulla, the collecting ducts again coalesce successively. A schematic diagram for the model is shown in Figure 1. Baseline single-nephron glomerular filtration rate (SNGFR) is set to 100 and 133 nl/min for the superficial and juxtamedullary nephrons, respectively, in both men and women. Assuming a total of 1 million nephrons in each kidney, this yields a single-kidney GFR of 105 mL/min.

The model accounts for the following 15 solutes: Na^+, K^+, Cl^-, HCO_3^-, H_2CO_3, CO_2, NH_3, NH_4^+, HPO_4^{2-}, $H_2PO_4^-$, H^+, HCO_2^-, H_2CO_2, urea, and glucose. The model is formulated for steady state and consists of a large system of coupled ordinary differential equations and algebraic equations (see model equations below). Model solution describes luminal fluid flow, hydrostatic pressure, luminal fluid solute concentrations and, with the exception of the descending limb segment, cytosolic solute concentrations, membrane potential, and transcellular and paracellular fluxes.

In this study, we develop an analogous multi-nephron model for a woman. We follow the approach implemented in our recent studies (Hu et al., 2019; Hu et al., 2020) in which we formulated sex-specific epithelial cell-based models of solute transport along the nephrons of the male and female rat kidneys. The male and female multi-nephron models presented here account for sex differences in the expression levels of apical and basolateral transporters (Veiras et al., 2017; Sabolic et al., 2012).

Key model equations

Conservation in the cellular and paracellular compartments. As shown in Figure 1, individual nephron segments have distinct morphological and transport properties, and are identified by the index i (i = PCT, S3, etc.). Consider a given nephron segment i at steady state. Conservation of water is described separately in the cellular and paracellular compartments (denoted by the subscripts 'C' and 'P', respectively), based on fluxes across individual membranes:

$$J^i_{v,LC} + J^i_{v,BC} + J^i_{v,PC} = 0 \quad \text{(Equation 1)}$$

$$J^i_{v,LP} + J^i_{v,BP} + J^i_{v,CP} = 0 \quad \text{(Equation 2)}$$

where $J^i_{v,ab}$ denotes transmembrane water flux from compartment a to compartment b, and the subscripts 'L' and 'B' denote lumen and blood, respectively. Conservation of mass for a non-reacting solute k takes a similar form:

$$J^i_{k,LC} + J^i_{k,BC} + J^i_{k,PC} = 0 \quad \text{(Equation 3)}$$

$$J^i_{k,LP} + J^i_{k,BP} + J^i_{k,CP} = 0 \quad \text{(Equation 4)}$$

where $J^i_{k,ab}$ is the transmembrane flux of solute k from compartment a to compartment b. For reacting solutes, conservation is imposed on total buffers. In the cellular and paracellular compartments (m = 'C' or 'P'):

$$\hat{J}^i_{CO_2,m} + \hat{J}^i_{HCO_3^-,m} + \hat{J}^i_{H_2CO_3,m} = 0 \quad \text{(Equation 5)}$$

$$\hat{J}^i_{A,m} + \hat{J}^i_{B,m} = 0 \quad \text{(Equation 6)}$$

where $\hat{J}^i_{k,m}$ is the net flux of solute k into compartment m, i.e., $\hat{J}^i_{k,C} \equiv J^i_{k,LC} + J^i_{k,BC} + J^i_{k,PC}$ and $\hat{J}^i_{k,P} \equiv J^i_{k,LP} + J^i_{k,BP} + J^i_{k,CP}$. Equation 6 is applied to buffer pair (A,B) which may be (HPO_4^{2-},$H_2PO_4^-$), (NH_3, NH_4^+), or (HCO_2^-, H_2CO_2). Buffer protonation reactions are generally sufficiently rapid to be taken at equilibrium; thus,

$$pH^i_m = pK_{HCO_3^-} + \log\frac{C^i_{HCO_3^-,m}}{C^i_{H_2CO_3,m}} \quad \text{and} \quad pH^i_m = pK_A + \log\frac{C^i_{A,m}}{C^i_{B,m}} \quad \text{(Equation 7)}$$

where $C^i_{k,m}$ denotes the concentration of solute k in compartment m of segment i. Finally, protons must also be conserved:

$$\sum_k \hat{J}^i_{k,m} = 0 \quad \text{(Equation 8)}$$

where the summation k is taken over H^+, NH_4^+, $H_2PO_4^-$, H_2CO_3, and H_2CO_2.

Conservation in lumen. We first consider mass conservation in the lumen of a nephron segment i that does not coalesce, i.e., we consider segments other than the connecting tubule and the inner-medullary collecting duct. In the lumen of such segments, conservation of water and non-reacting solutes is given by

$$\frac{dQ^i}{dx} = 2\pi r^i \hat{J}^i_{v,L} \quad \text{(Equation 9)}$$

$$\frac{d}{dx}\left(Q^i C^i_{k,L}\right) = 2\pi r^i \hat{J}^i_{k,L} \quad \text{(Equation 10)}$$

where Q^i denotes the volume flow. $\hat{J}^i_{v,L} \equiv J^i_{v,LC} + J^i_{LP}$ denotes the total water flux (i.e., transcellular plus paracellular); $\hat{J}^i_{k,L}$ is defined similarly. For reacting solutes, conservation is applied to total buffers:

$$\frac{d}{dx}\left(Q^i C^i_{CO_2,L} + Q^i C^i_{HCO_3,L} + Q^i C^i_{H_2CO_3,L}\right) = \hat{J}^i_{CO_2,L} + \hat{J}^i_{HCO_3,L} + \hat{J}^i_{H_2CO_3,L} \quad \text{(Equation 11)}$$

$$\frac{d}{dx}\left(Q^i C^i_{A,L} + Q^i C^i_{B,L}\right) = \hat{J}^i_{A,L} + \hat{J}^i_{B,L} \quad \text{(Equation 12)}$$

For the coalescing segments, i.e., the connecting tubule and inner-medullary collecting duct, water and solute flows are scaled by the tubule population ω^i. That is, ω^i denotes the fraction of tubule i remaining at a given spatial location. As such, Eqs. 9 and 10 become

$$\frac{d}{dx}\left(\omega^i Q^i\right) = \hat{J}^i_{v,L} \quad \text{(Equation 13)}$$

$$\frac{d}{dx}\left(\omega^i Q^i C^i_{k,L}\right) = \hat{J}^i_{k,L} \quad \text{(Equation 14)}$$

Eqs. 11 and 12 are modified similarly. The model assumes that the fraction of connecting tubules ω^{CNT} remaining at coordinate x^{CNT} is given by

$$\omega^{CNT}\left(x^{CNT}\right) = 2^{-3.32\ x^{CNT}/L^{CNT}} \quad \text{(Equation 15)}$$

where L^{CNT} represents the connecting tubule length and x^{CNT} is the distance from its entrance. The parameters are chosen so that the convergence of connecting tubules within the cortex yields a 10:1 ratio of loop-to-cortical collecting duct; i.e., $\omega^{CNT}(L^{CNT}) = 0.1$, indicating that 10% of the connecting tubules remain at the connecting with the cortical collecting ducts.

Similarly, the collecting ducts coalesce within the inner medulla, according to

$$\omega^{IMCD}\left(x^{IMCD}\right) = 0.1 \times \left(1 - 0.95\left(\frac{x^{IMCD}}{L^{IMCD}}\right)^2\right) e^{-2.75\ x^{IMCD}/L^{IMCD}} \quad \text{(Equation 16)}$$

where L^{IMCD} represents the length of the inner-medullary collecting duct and x^{IMCD} is the distance from its entrance.

Fluid pressure, tubular flow, and flow-dependent transport. Tubular fluid flow is described by the pressure-driven Poiseuille flow, where hydrostatic pressure P^i is related to volume flow Q_i and luminal radius r_i by

$$\frac{dP^i}{dx} = -\frac{8\mu Q^i}{\pi\left(r^i\right)^4} \quad \text{(Equation 17)}$$

where μ is the luminal fluid viscosity (6.4×10^{-6} mmHg.s^{-1}).

Flow-dependent transport is represented along the proximal tubule, where reabsorption has been reported to vary proportionally with SNGFR in mammals (Schenermann et al., Pflüger Arch. 1968). Thus, we assume that the proximal tubule is compliant, with luminal radius r^{PT} dependent on tubular pressure P^{PT} as

$$r^{PT} = r_0^{PT}\left(1 + \nu^{PT}\left(P^{PT} - P_0^{PT}\right)\right) \quad \text{(Equation 18)}$$

where the reference radius $r_0{}^{PT}$ is chosen to be 14 μm, the reference pressure $P_0{}^{PT}$ is chosen to be 20 mmHg, and the tubular compliance ν^{PT} is taken as 0.02. Once r^{PT} is determined, we can compute microvillous torque τ^{PT} which modulates transporter density:

$$\tau^{PT} = \frac{8\mu\ Q^{PT} l^{PT,mv}}{\left(r^{PT}\right)^2}\left(1 + \frac{l^{PT,mv} + \delta^{PT,mv}}{r^{PT}} + \frac{\left(l^{PT,mv}\right)^2}{2\left(r^{PT}\right)^2}\right) \quad \text{(Equation 19)}$$

where $l^{PT,mv}$ is the microvillous length taken as 2.5 μm, and $\delta^{PT,mv}$ is the height of the microvillous tip taken as 0.15 μm. Transporter density is then scaled by

$$1 + s\left(\frac{\tau^{PT}}{\tau_0^{PT}} - 1\right) \quad \text{(Equation 20)}$$

where the reference torque $\tau_0{}^{PT}$ is computed using Equation 3 with Q^{PT} set to SNGFR. The scaling factor s is set to 1.3 and 0.65 for the proximal convoluted tubule segment and the S3 segment, respectively. Downstream of the proximal tubule, nephron segments are assumed to be rigid and tubular transport is assumed to be independent of fluid flow.

Flux calculations. Volume flux $J^i_{v,ab}$ is calculated from the osmotic and hydraulic pressure

$$J^i_{v,ab} = A^i_{ab} L^i_{p,ab}\left(\sigma^i_{ab}\Delta\pi^i_{ab} + \Delta P^i_{ab}\right) \quad \text{(Equation 21)}$$

where A^i_{ab} is the membrane area, $L^i_{p,ab}$ denotes the hydraulic permeability, σ^i_{ab} denotes the reflective coefficient, $\Delta\pi^i_{ab} \equiv RT\sum\Delta C^i_{ab}$ is the osmotic pressure gradient computed in terms of the osmolality

difference $\Sigma\Delta C^{i}_{ab}$ and the product of the ideal gas constant R with the thermodynamic temperature T, and ΔP^{i}_{ab} is the hydrostatic pressure gradient.

Transmembrane solute flux may include a number of components, depending on the solute, such as electrodiffusion, coupled transport across cotransporters and/or exchangers and primary active transport across ATP-driven pumps. Electrodiffusive fluxes for ions are given by the Goldman-Hodgkin-Katz equation:

$$J^{i}_{k,ab} = A^{i}_{ab}\,\rho^{i}_{k,ab}\frac{z_k F\,\Delta V^{i}_{ab}}{RT}\,\frac{C^{i}_{k,a} - C^{i}_{k,b}\exp\left(-z_k F\,\Delta V^{i}_{ab}/RT\right)}{1-\exp\left(-z_k F\,\Delta V^{i}_{ab}/RT\right)} \qquad \text{(Equation 22)}$$

where $\rho^{i}_{k,ab}$ is the membrane permeability, z_k is the solute valence, F is Faraday's constant, and ΔV^{i}_{ab} denotes the electrical potential gradient. For an uncharged solute, the corresponding flux is:

$$J^{i}_{k,ab} = A^{i}_{ab}\,\rho^{i}_{k,ab}\left(C^{i}_{k,ab} - C^{i}_{k,ab}\right) \qquad \text{(Equation 23)}$$

Model parameters. Nephron segment lengths and luminal diameters in the human kidney are summarized in Table S1; additional model parameters can be found in (Layton and Layton, 2019). Key differences in nephron transport parameters between men and women are summarized in Table 1. The model is implemented in Python.